J. Appl. Cryst. (1999). **32**, 65–70

Calibration of spiral-readout image-plate detectors

Mark A. White, Stanley J. Watowich and Robert O. Fox

X-ray Crystallography Center, Sealy Center for Structural Biology, Department of HBC&G, University of Texas Medical Branch at Galveston, Galveston, Texas 77555, USA. E-mail: fox@bloch.utmb.edu

(*Received 9 February 1998; accepted 3 August 1998*)

Abstract

An improved method for intensity-uniformity calibration of diffraction data collected on spiral-readout image-plate (IP) systems is described. This technique is applicable to all types of spiral-readout IP detectors. The procedure utilizes an attenuated direct-beam scan of the IP to generate a radial-sensitivity calibration table. Exposure and scanning of the calibration frame are done on the same time scale as typical data collections, and require no additional equipment. Specific examples are presented for use with Mac Science DIP2000 systems. The new radial calibration is shown to reduce significantly structure-based R factors. The improved radial calibration is also shown to lower $R_{\rm merge}$ when the IP is offset from the beam center. In addition to improving data quality and statistics, this method provides a quick and simple diagnostic tool to monitor changes in the sensitivity of the IP detector as a function of age.

1. Introduction

Image-plate (IP) scanners have proven ideally suited for collecting diffraction data from powders, small molecules, macromolecules, viruses, and even for small-angle and time-resolved diffraction (Amemiya, 1995; Miyahara *et al*., 1986). Image plates have found general acceptance and widespread use largely because of their high sensitivity, low intrinsic noise, high uniformity (∼2%), high accuracy (∼1%), large dynamic range ($>10^6$), large apertures and spatial resolution [∼170 μm (FWHM) point spread function], and relatively long-lived image ($\tau_1 \simeq 0.7$ h) (Amemiya, 1995).

Notwithstanding these many advantages offered by IP systems, the problem of calibrating the diffraction data remains. Most IP detectors and all multiwire (MW) and charge-coupled device (CCD) area detectors require some type of sensitivity calibration to correct the intensity measurements in their image files. Although this is most commonly associated with spiral-readout IP systems, there are several linear-type readout IP systems which use an internal sensitivity calibration to correct their intensities (Molecular Dynamics, Sunnyvale, CA, USA; Fuji, Stamford, CT, USA). Furthermore, both CCD-based systems and MW area detectors require an image spatial-distortion correction in addition to this sensitivity calibration in order to be suitable for collecting X-ray diffraction data.

There are three commonly used varieties of IP scanner: (i) flat rectangular scanners such as the Fuji BAS 2000, the Molecular Dynamics Phosphor Imager and the Rigaku R-Axis II, (ii) helical or spinning-head IP scanners like the Mac Science DIP320, DIP3000 and the Rigaku R-Axis IV, and (iii) spiral-readout or rotating IP disc scanners. Common spiral-readout scanners include the Mar Research MAR series, the Mac Science DIP2000 series and the Stoe scanner. The MAR scanner uses a variable-speed readout which produces a constant area per measurement (Mar Research, 1992). The DIP uses a simpler constant-speed IP rotation (Tanaka *et al*., 1990). In the DIP scanner the area per measurement and therefore the sensitivity varies with radius. This variation in sensitivity is corrected by the measurement software using a factory-calibrated look-up table. A side effect of this over-sampling (combining many actual measurements into one measurement or pixel) of the image near the center of the IP is an increase in the dynamic range of the detector to beyond 10^6 and a systematic background shift inversely proportional to the radius and proportional to the A/D (analog to digital) electronic offset. The MAR scanner also requires a correction look-up table. Although measurements with the MAR scanner are made at constant area, there is still a variation in the sensitivity across the IP. The source of these variations has not been discussed in the literature.

Several different methods have been used to calibrate the sensitivity of area detectors, the most common being some variation on the flood-field correction. Flood-field methods, which use a radioactive point source (Blum *et al*., 1987; Tanaka *et al*., 1990; Mar Research, 1992; Moy *et al*., 1996), X-ray fluorescent sample (Katayama, 1996; Siemens, 1996) or a radiological X-ray tube (Fuji), do not permit a background reference to be collected simultaneously with the exposure, and require either a hazardous radioactive source, a special X-ray fluorescent foil, or a flood X-ray tube. The method described here permits simultaneous recording of the background and signal, requires no additional items and poses no additional safety hazard.

ISSN 0021-8898

Although all data presented in this paper were collected on a Mac Science DIP2030, the methodology and results should be applicable to other spiral-readout systems.

2. Materials and methods

The calibration of the radial sensitivity of the Mac Science DIP2000 series area detectors is stored in a look-up table (named \$XDIPHOME/Xdipsys/data/CorrectData). As delivered from the factory, this table is generated from a polynomial fit to fewer than 100 data points evenly distributed along a radial arc (Katayama, 1995). The original factory method required that the user attenuate the direct beam with filters supplied with the mirror system or monochromator, and make up to 99 direct-beam exposures with the IP at different positions. We have found that this polynomial fit poorly describes the radial variation in sensitivity at the two extremes of small or large radius. We have therefore attempted to replace this fit with an empirical correction table generated from more than 2000 data points of various radii (White, 1997). Mac Science has recently switched from the individual direct-beam exposures to a flood-field exposure using an amorphous Fe X-ray fluorescent sample. However, the final calibration table is still produced from a polynomial fitting function (Katayama, 1996) rather than by the empirical method presented here.

Rather than using individually integrated points along the IP's arc of motion, we utilize a continuous line of data points. By using the internal IP exchange motion the IP arm is moved into and out of the attenuated (0.125 mm Ni filter) X-ray beam, at constant speed, several times (10–20). Thus we are able to generate a narrow arc of constant exposure from the lower edge of the IP through the center to a position of 30° (10 cm) above the center of the 30 cm IP (Fig. 1*a*). The *DIP-Xpress* software and a modified data-collection script file (\$DIPHOME/Xdipsys/conf/DIP2030.SUB) are used to control the motion of the IP arm, exposure and readout. This calibration frame is collected automatically and in the same sequence as a typical data collection. Only the exposure segment of the procedure has been altered to produce a narrow arc of constant X-ray exposure on the IP and the factory-installed radial correction table was replaced with a null (constant) 'CorrectData' table.

On MAR systems, the linear translation of the 2θ offset accessory could be used to create a line exposure. Alternately an ^{55}Fe source and pinhole mask could be attached to the readout arm, and this arm scanned across the IP several times to create the calibration exposure.

After exposure the calibration image is automatically scanned and recorded to disk. The calibration image file is then processed using the C software routine *RC.Scan.c*. This program integrates the arc, removing any background contribution to the intensity [see equation (1)].

The integrated intensity at a radius $r(j)$ is

$$I[r(j)] = \left[\sum_{i=i_o-N/2}^{i=i_o+N/2} \mathrm{IP}(i,j) - \sum_{i=i_o-N}^{i=i_o-N/2} \mathrm{IP}(i,j) - \sum_{i=i_o+N/2}^{i=i_o+N} \mathrm{IP}(i,j)\right] \times [1 - (R_a - R + i_o)/R_a] \quad (1)$$

where i_o (pixels) and $r(j)$ (mm) are given by

$$i_o = R - R_a + [R_a^2 - (R-j)^2]^{1/2}$$

and

$$r(j) = 0.1[(R-i_o)^2 + (R-j)^2]^{1/2}$$

where R is the IP radius and R_a the readout-arm radius, both in pixels.

The oversampling spiral readout has an additional artefact which should be removed, a nonuniform systematic electronic zero-point offset which varies inversely with IP radius. This electronic zero-point offset is the result of the variable $(1/r)$ area per measurement

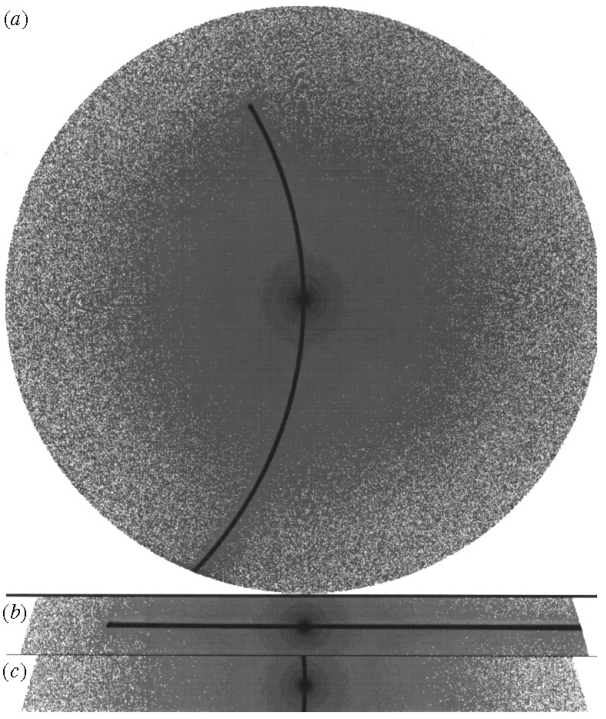

Fig. 1. Direct-beam exposure of the IP. (*a*) The attenuated direct-beam exposure of the IP recorded on the DIP2030. The plate exchange mechanism of the DIP2030 was used to move the IP through the beam at a constant rate. Note that the center of the IP has a larger background as a result of the oversampling at smaller radius. Below the main image are shown (*b*) the calibration arc and (*c*) the background or orthogonal arc created by the *RC.Scan.c* program for integration.

(oversampling) of the readout combined with a nonzero A/D offset and produces a systematic background signal with a $1/r$ dependence. This systematic background signal has a strong effect on the measurement at small r and cannot easily be removed from flood-field-type calibrations. The small exposure area, a fine (0.5 mm wide) arc rather than a flood field, means that the background intensity can be measured from an 'orthogonal' arc in the same image used to measure the sensitivity, as shown in Figs. 1(*c*) and 1(*b*), respectively. The background as measured by this 'orthogonal' arc is given by (1) with $I(r) \rightarrow B(r)$, $i \rightarrow j$ and $j \rightarrow i$. Therefore the sensitivity as a function of radius is

$$S(r) \propto I(r) - B(r) \tag{2}$$

where

$$B(r) = \left[\sum_{j=i_o-N/2}^{j=i_o+N/2} \mathrm{IP}(j, i_o) - \sum_{j=i_o-N}^{j=i_o-N/2} \mathrm{IP}(j, i_o) - \sum_{j=i_o+N/2}^{j=i_o+N} \mathrm{IP}(j, i_o)\right] \times [1 - (R_a - R + i_o)/R_a].$$

This calibration method utilizes data which are collected in the same cycle (exposure and scan) time as a typical data-collection frame (~10 min), and which therefore have similar effects arising from image decay (Graafsma, 1994; Amemiya, 1995) and background fogging. Different researchers have reported varying decay rates for the IP image dependent on the type of phosphor and temperature. Our measurements on the DIP2030 show a double exponential decay similar to that reported by other researchers, but with faster decay rates [see equation (3)] of $\tau_1 = 20$ (4) min as compared with $\tau_1 = 30$ or 40 min previously reported (Graafsma, 1994; Amemiya, 1995). The faster decay rate could be due to the higher sensitivity of the newer Fuji phosphors and/or the warmer environment of the enclosed online IP scanner. Previous measurements stored the phosphor at room temperature (297 K) during and after exposure and were scanned with an offline scanner. The IP image decay measured for the DIP2030 is

$$I(t) = I(0)\{0.20\,(2)\exp[-t/20\,(4)] + 0.80\,(2)\exp[-t/4400\,(600)]\} \tag{3}$$

where t is in min.

Since the fast component of the image decay is of the same order of magnitude as the cycle time (7 min) it is important that the readout process for the calibration closely matches that used in a typical data collection.

The narrow exposed arc is scanned in a closer approximation to a normal reflection peak, as compared to the constant intensity of the flood-field method: the arc is read out as a sharp peak in the scan direction with a rise and fall time similar to that of a typical reflection. In addition, the peak intensity is approximately 15 000 A/D units and is therefore recorded only on the high-sensitivity photomultiplier where the majority of X-ray diffraction data is measured. This choice avoids any scale changes between the two photomultipliers that might affect the radial calibration. The crossover point between the two photomultiplier tubes on the DIP2030 is between 24 000 and 32 768 counts per pixel. A peak intensity between 12 000 and 20 000 counts per pixel is below the crossover region while providing statistically useful data.

A disadvantage of this orthogonal-arcs method is that at the very center of the IP, where the two arcs cross, the method breaks down. This leaves a small gap of about 30 pixels (3 mm) diameter in the calibration at the center of the IP. However, this is not a serious matter for two reasons: the area is very small and it is not normally used for collecting diffraction data since it is behind the beamstop. Our software masks out this area in the final calibration table, as is done with the MAR scanners, which cannot scan the center of the IP.

After exposure and integration (*RC.Scan.c*) of the calibration image to produce a calibration table, this table of data is then imported into an *Excel* (Microsoft) spreadsheet. The data points at the edge of the IP and the +30° turn-around point are removed from the table and the table is sorted by radius and smoothed. Smoothing is done by averaging ±50 points at each radius. The table output from *Excel* is then used by the program *RC.CorrectData.c* to create the new 'Correct-Data' image file for the data-collection software. New versions of the programs *RC.Scan.c* and *RC.Correct-Data.c* are being written which will take one or several calibration images and automatically integrate, trim, average and smooth the data and then write a new radial calibration file.†

2.1. *Crystallographic data collection and refinement*

X-ray diffraction data from a Y27W Ca^{2+} pdTp nuclease mutant crystal ($0.5 \times 0.16 \times 0.15$ mm) were collected to 1.8 Å on a Mac Science DIP2030H area detector at 278 K, in a combination of 125 0.5° frames at a χ of 0° and 44 1° frames at a χ of 30°. The frames processed using *DENZO/SCALEPACK* were 96.6% complete with an overall R_{merge} of 5.2% (20–1.9 Å). After processing in *DENZO* the intensities were corrected using *RC.Scalepack.exe*. The structure refinement started as a molecular-replacement problem with 1stn.pdb (Hynes & Fox, 1991; Bernstein *et al.*, 1977) as a starting model for the protein and 1kaa.pdb (Hodel *et al.*, 1993) for the ligands. After several rounds of model building in *XtalVIEW* (McRee, 1992) and *X-PLOR* (Brünger, 1992*a*), the final model was refined with 9163

† IP decay data and the software source code are available from the IUCr electronic archives (Reference: MF0016). Services for accessing these data are described at the back of the journal.

($F > 2\sigma$) reflections to an $R_{\rm cryst}$ of 18.6% (8–1.9 Å) with the new calibration.

X-ray diffraction data from an H124C nuclease mutant crystal (0.6 × 0.45 × 0.4 mm) were collected to 2.0 Å on a Mac Science DIP2030H area detector at 273 K, in 85 1.5° frames. The frames processed using *DENZO*/*SCALEPACK* were 98.2% complete with an overall $R_{\rm merge}$ of 3.2% (20–2.0 Å). After processing in *DENZO* the intensities were corrected using *RC.Scalepack.exe*. The structure refinement started as a molecular-replacement problem with 1stn.pdb as a starting model. After several rounds of model building in *XtalVIEW* and *X-PLOR*, the final model was refined with 9370 ($F > 2\sigma$) reflections to an $R_{\rm free}$ of 24.2% and $R_{\rm cryst}$ of 18.0% (8–2.0 Å) with the new calibration.

3. Results

A radial calibration table is used by the DIP2030 IP scanner to correct its intensity measurements for variation in the detector sensitivity across the IP. This is a simple radial function. We have attempted to measure the accuracy of the recalibrated intensities and to create our own empirical calibration table, improving upon the factory-installed calibration. The method of measuring the accuracy of the installed calibration and the method of measuring a new calibration are identical: only the table used to correct the intensities is changed. This method involves exposing the IP to an attenuated direct beam, while a special command script moves the IP, so that an arc of constant exposure, from the edge of the IP through the center, is created (Fig. 1).

After generating the new calibration the next step in the calibration process is to measure the accuracy of both the factory calibration and the new calibration by exposing the IP to an attenuated X-ray beam, using a special command script. The exposure made with the factory calibration shows significant systematic variations of up to 15% from a flat calibrated response (Fig. 2*a*). The response with the new calibration (Fig. 2*b*), derived from the sensitivity curve (Fig. 2*c*), has within measurement error a flat calibrated response over the majority of the IP. In the region where diffraction data are collected, the response of the new calibration has less than ±0.5% systematic deviation. Near the center of the IP, $r < 5$ mm, the new calibration still has significant deviation from the ideal. However, this region is not generally used for data collection unless the plate is offset. The outer edge of the IP has significant deviation from the ideal for both calibrations, which may be caused by damage to the IP phosphor edge during manufacturing. The large differences (>10%) between the new calibration and the factory calibration, particularly near the center and edge of the IP, are shown by the ratio of the factory and new radial calibration tables in Fig. 3. The significance of these calibration differences for $R_{\rm cryst}$, $R_{\rm free}$ and $R_{\rm merge}$ will be discussed below.

The new calibration method produces a simple radial-dependent calibration factor. The correlation between IP radius and the Bragg d spacing, for zero offset IPs, means that the radial calibration will always be the same for symmetry-equivalent reflections [see equation (4)]. Therefore the calibration can also be applied after scaling and merging of the data. This allows a direct comparison of the quality of the calibration in terms of $R_{\rm cryst}$. The recalibrated reflection intensities are given by

$$I(hkl)_{\rm recalibrated} = S(r)I(hkl) \qquad (4)$$

where

$$r = D\tan\{a\sin[\lambda/2d(hkl)]\}.$$

D is the detector distance and $d(hkl)$ is the Bragg d spacing of reflection hkl.

The program *RC.Scalepack.c* uses the ratio of the new calibration to the old calibration, shown in Fig. 3, to recalibrate the intensities measured using the old factory-installed calibration file. This was done for data of several nuclease (staphylococcal nuclease) mutants (White *et al.*, 1998) that were collected prior to instal-

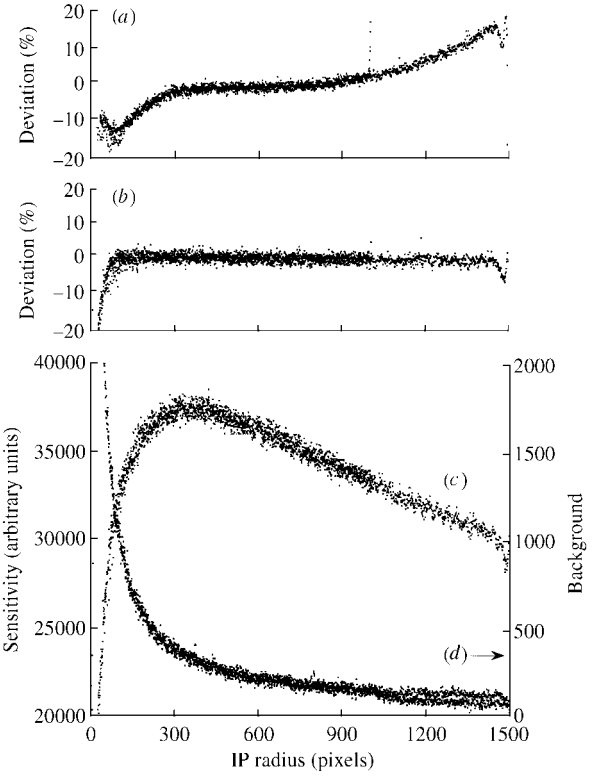

Fig. 2. Calibrated response curves for DIP2030. A comparison of the per cent deviation of the calibrated IP response for (*a*) the original factory calibration and (*b*) the new calibration. The lower plot (*c*) shows the measured sensitivity data for the new calibration prior to trimming, sorting and smoothing. The lower curve (*d*) is the $1/\tau$ systematic background shown on an expanded scale for comparison. Note that the overexposed turn-around point at +30° ($r \simeq 1020$) has not been removed from the data in (*a*).

lation of the new calibration table. Two of these mutants were refined using both the original and recalibrated data, thus permitting a direct comparison of the calibration effect on crystal structure and refinement.

Table 1 shows the results of applying the new calibration to two nuclease mutant data-sets. The crystallographic R factor of the Y27W mutant significantly decreased from 22.5% to 18.6%. This demonstrates that the systematic errors in the factory calibration table cannot be modeled by the B factors and are a significant source of error in the structure refinement.

The effect of the new radial calibration on the $R_{\rm free}$ (Brünger, 1992*b*) of the H124C nuclease mutant was most dramatic and demonstrative of the need for an accurate radial calibration. Prior to application of this new calibration the $R_{\rm free}$ of the refined H124C structure had been abnormally high. The $R_{\rm free}$ of 42.9% (8–2 Å) after initial rigid-body refinement indicated a serious problem with the data. The $R_{\rm free}$ of 37.1% for the refined structure, including 30 waters, was not considered acceptable. Moreover, this refinement demonstrated a great instability in the refinement of the B factor. After applying the new radial calibration function to the scaled and merged reflection intensities, the initial $R_{\rm free}$ decreased from 42.9% to 25.8%. The structure with 36 waters refined to a final $R_{\rm free}$ of 24.7%, and a crystallographic R factor of 18.6% with reasonable B values.

The effect of the new calibration on R factors of the H124C mutant was even greater than for the Y27W mutant. The reason for this is that the Y27W crystal was significantly smaller and diffracted to only 1.9 Å, as opposed to ~1.6 Å for the H124C mutant crystal. Also, the Y27W mutant did not diffract to the edge of the IP (1.8 Å). Therefore, no data were collected in the region of the IP where the change in the calibration table is the largest, and only weak (3σ at 1.9 Å) data were collected in the region of the IP where there are moderate differences between the two calibrations. The H124C mutant had an average of 20σ reflections at the IP edge (2.0 Å), where the calibration differences are the largest, and therefore shows the greatest improvement in R factors. This is evidence of the strong relationship between the accuracy of the radial calibration function and the quality of the final structure.

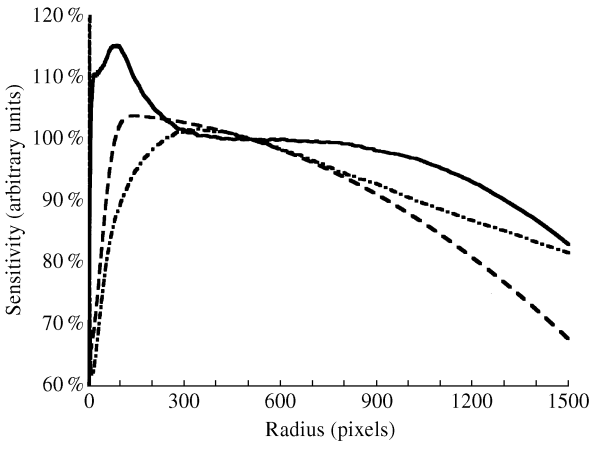

Fig. 3. Calibration tables for the DIP2030. The ratio (—) of the factory (- - -) default CorrectData table and the new (- · -) CorrectData tables is used by the software routine *RC.Scalepack.c* to correct previously scaled and merged data which were collected prior to installation of the new calibration table. The calibrations are scaled to 100% at $r = 500$ pixels, which is approximately in the center of the flat region for the ratio of the two curves.

In many diffraction experiments the X-ray beam center is orthogonal to the IP and intersects the center of the IP: an IP 2θ offset of 0°. In this geometry, symmetry-equivalent reflections, which are used to calculate interframe scale factors and $R_{\rm merge}$, are collected at the same IP radius. Since the same calibration scale function $S(r)$ is applied to all symmetry-related reflections, the radial calibration function will not affect the scale factors or the $R_{\rm merge}$. However, when the IP is offset, so that the X-ray beam center is no longer at the center of the IP, the radial calibration scale factor for symmetry-related reflections will not generally be equivalent. Therefore, the interframe scale factors and $R_{\rm merge}$ will be affected by the radial calibration scale factor when the IP is offset from $2\theta = 0°$.

To test the effect of the new calibration on $R_{\rm merge}$, a partial data-set of thaumatin I sweet protein (De Vos *et al.*, 1985) was collected with the IP offset by 30° (+10 cm vertical offset, $D = 100$ mm) and with a null (constant) CorrectData calibration table. The program *RC.Image.c* applied the two different calibrations to the image frames prior to processing with *DENZO* (Otwinowski & Minor, 1998). Thus the two calibrations were independently applied to exactly the same diffraction data. These two data-sets were then processed with *SCALEPACK*. The $R_{\rm merge}$ (60–2.0 Å), for each calibration, is shown in Table 1. The new calibration resulted in a significant improvement in $R_{\rm merge}$ for this data-set, from 3.5% for data processed with the factory-supplied calibration to 3.1% for data processed with the new calibration. The resulting calibration correction would be even larger if the data were collected without alignment of a mirror plane of symmetry, which in this case resulted in similar radii for many merged reflections. These measurements caution against using the $R_{\rm merge}$ or other symmetry-related statistical tests to determine the quality of data produced by a detector. This insensitivity of $R_{\rm merge}$ to resolution-related systematic errors must be considered in addition to its well known inverse relationship to data quality when the number of independent measurements is small (Gewirth, 1995; Weiss & Hilgenfeld, 1997).

4. Conclusions

An improved method for the calibration of spiral-readout image-plate scanners has been presented. This method is simple to use and requires no additional

Table . *Effect of radial calibration on R factors*

	Standard calibration		New calibration	
	$R_{\rm cryst}$ (%)	$R_{\rm free}$ (%)	$R_{\rm cryst}$ (%)†	$R_{\rm free}$ (%)†
Nuclease Y27W structure (1.9 Å)	22.5	NA	18.6	NA
Nuclease H124C structure: rigid-body refinement (2.0 Å)	29.7	42.9	21.7	25.8
H124C: final structure (2.0 Å)	24.9	37.1	18.0	24.2
	$R_{\rm merge}$ (%)‡		$R_{\rm merge}$ (%)‡	
Thaumatin I: offset data $R_{\rm merge}$ (2.0 Å)	3.5			3.1

† The calibration was applied to the merged and scaled reflection intensities using *RC.Scalepack.c*. $R_{\rm cryst} = \sum_{hkl} |F_{\rm obs} - F_{\rm calc}| / \sum_{hkl} F_{\rm obs}$, $R_{\rm free} = \sum_{hkl} |F_{\rm cv} - F_{\rm calc}| / \sum_{hkl} F_{\rm cv}$, where $F_{\rm cv}$ is a (10%) subset of the data removed from $F_{\rm obs}$.
‡ The data were collected without any calibration. The calibration tables were then applied to the images by *RC.image.c* to create two data-sets from one data collection. The $R_{\rm merge}$ ($R_{\rm merge} = \sum_h |I_h - \langle I_h \rangle| / \sum_h \langle I_h \rangle$) was then calculated separately for each calibration using *DENZO/SCALEPACK*.

equipment. The new radial-calibration method has been demonstrated to improve significantly the quality of structures, as measured by $R_{\rm free}$ and $R_{\rm cryst}$, refined with data obtained from a spiral-readout IP detector. The $R_{\rm merge}$ was also shown to be lowered in the case of nonzero IP 2θ offset. We recommend that all users of spiral image-plate scanners use this technique to check the calibration of their detector on a regular basis.

The authors are grateful to Deqian Liu who supplied all the crystals used in these experiments and to Dr Edmund W. Czerwinski who translated *RC.Scalepack.c* into Fortran. This work was supported by the Welch Foundation and the Sealy and Smith Foundation.

References

Amemiya, Y. (1995). *J. Synchrotron Rad.* **2**, 13–21.
Bernstein, F. C., Koetzle, T. F., Williams, G. J., Meyer, E. E. Jr, Brice, M. D., Rodgers, J. R., Kennard, O., Shimanouchi, T. & Tasumi, M. (1977). *J. Mol. Biol.* **112**, 535–592.
Blum, M., Metcalf, P., Harrison, S. C. & Wiley, D. C. (1987). *J. Appl. Cryst.* **20**, 235–242.
Brünger, A. T. (1992*a*). *X-PLOR Manual*, Version 3.1. New Haven, CT: Yale University Press.
Brünger, A. T. (1992*b*). *Nature* (*London*), **335**, 472–475.
De Vos, A. M., Hatada, M., Van der Wel, H., Krabbendam, H., Peederman, A. F. & Kim, S. H. (1985). *Proc. Natl Acad. Sci. USA*, **82**, 1406–1409.
Gewirth, D. (1995). *The HKL Manual. A Description of the Programs DENZO, XDISPLAYF and SCALEPACK*, 4th ed., pp. 93–96. New Haven, CT: Yale University Press.
Graafsma, H. (1994). Personal communication.
Hodel, A., Kautz, R. A., Jacobs, M. D. & Fox, R. O. (1993). *Protein Sci.* **2**, 838–850.
Hynes, T. R. & Fox, R. O. (1991). *Proteins Struct. Funct. Genet.* **10**, 92–105.
Katayama, C. (1995). Personal communication.
Katayama, C. (1996). *DIP*2000 *User Manual*, Section 5. Mac Science Co. Ltd, 1-5-1 Shinyokohama, Kohoku-ku, Yokohama, Kanagawa, 222, Japan.
McRee, D. E. (1992). *J. Mol. Graphics*, **10**, 44–46.
Mar Research (1992). *Imaging Plate Detector System*. X-ray Research Gmbh, Luruper Hauptstrasse 50, 2000 Hamburg 5J, Germany.
Miyahara, J., Takahashi, K., Amemiya, Y., Kamiya, N. & Satow, Y. (1986). *Nucl. Instrum. Methods*, A**246**, 572–578.
Moy, J. P., Hammersley, A. P., Svenson, S. O., Thompson, A., Brown, K., Claustre, L., Gonzalez, A. & McSweeny, S. (1996). *J. Synchrotron Rad.* **3**, 1–5.
Otwinowski, Z. & Minor, W. (1998). *The HKL Program Suite*. In preparation.
Siemens (1996). *SMART Software Reference Manual*, ch. 2. Siemens Analytical X-ray Systems Inc., Madison, WI, USA.
Tanaka, I., Yao, M., Mamoru, S., Hikichi, K., Matsumoto, T., Kozasa, M. & Katayama, C. (1990). *J. Appl. Cryst.* **23**, 334–339.
Weiss, M. S. & Hilgenfeld, R. (1997). *J. Appl. Cryst.* **30**, 203–205.
White, M. A. (1997). *X-ray Crystallography at the Sealy Center for Structural Biology, What's New*, http://www.hbcg.utmb.edu/xray/rc.html or via ftp://anonymous@xray.utmb.edu/pub/2030RC.